

NICKEL THIN FILMS GROWN BY PULSED LASER DEPOSITION: INFLUENCE OF SUBSTRATE AND SUBSTRATE TEMPERATURE

M. NAWAZ. RIZWAN^{a,*}, M. A. KALYAR^a, C. BELL^b, M. ANWAR-UL-HAQ^a,
A. R. MAKHDOOM^c

^a*Department of Physics, University of Sargodha, Sargodha 40100, Pakistan*

^b*School of Physics, University of Bristol, Tyndall Avenue, BS8 1TL, UK*

^c*Department of Natural Sciences and Humanities, Rachna College of Engineering
and Technology, University of Engineering and Technology, Lahore 54890,
Pakistan*

Nickel thin films were grown on glass and copper substrate in ultrahigh vacuum at energy density 2×10^{10} watt/cm² using Nd:YAG laser. XRD analysis showed the amorphous growth of thin film at low substrate temperature (T_s) while higher T_s supported crystalline growth. Magnetic moment, magnetic residual ratio and coercivity of thin films decreased with increase in T_s for both substrates. However, this decrease was sharp for films deposited on glass substrate as compared to that deposited on copper in T_s range 100°C-500°C. Electrical resistivity of thin film grown on glass substrate decreased while Hall carrier mobility increased with increase in T_s .

(Received July 30, 2020; Accepted November 14, 2020)

Keywords: Nickel thin films, Pulsed laser deposition, Vibrating sample magnetometer (VSM), Anisotropic magnetoresistance (AMR), Resistivity and carrier mobility

1. Introduction

Metallic thin film has become an initiative subject of interest in many fields of advance technologies such as electronic and micro-electronics. Ferromagnetic thin films have a few distinct characteristics like high flexibility and low electrical resistivity, among the other physical and mechanical properties. These specific properties make thin films an appropriate candidate for their applications in various fields of modern technology like photo-thermal energy conversion, micro-electronics, transparent electrodes and in devices used for bio-medical analysis [1].

Nickel is a fundamental transition metal, with high temperature stability, oxidation-resistance, corrosion and wear- resistance, and low electrical resistivity [2]. Owing these precise properties together with low cost and easy commercial availability, the popularity of nickel has been continuously increased during the past few decades. Furthermore, the ferromagnetic nature of nickel makes it more valuable for various topical fields such as photo thermal conversion, nanotechnology and magnetic resonance imaging [3]. The most important application of nickel is in the growth of thin film [4], which plays a key role in fabrication of essential components for the various technological fields based on the fabrication of nanostructured materials. Thin film produced by a suitable method under optimized deposition parameters may possess different optical, electrical, chemical and magnetic properties which are quite different of same properties of bulk materials [5]. Therefore, the domain of applications for nickel thin films has been widely increased due to their remarkable properties. Nickel thin films have found applications in many areas such as, ferro-fluid technology, magnetic-resonance imaging (MRI) [6-8], decorative-coating, corrosion- resistant coating [9], in microsystems and nuclear industry [10], nano-technology [12], solar-thermal energy conversion [10,12] and as catalyst for carbon nanotubes [13]. Ferromagnetic nickel thin films are also used in the preparation of magnetic-sensors, which have their applications in bio-systems, hard-drive disk of computes, and microelectro-mechanical systems [15]. The magnetic properties of nickel thin films are produced due to spin polarization of 3d electrons and

* Corresponding author: rizwannawazsial@yahoo.com

depend on the deposition method, growth parameters, microstructure, texture, substrate-temperature, type of substrate-material, thickness and grain size [3-4]. Several researchers have worked on the structural, physical and morphological properties of nickel thin films [10, 16-18].

Magnetic properties of nickel thin films deposited by RF magnetron sputtering [9], electron beam evaporation [14], thermal evaporation [13,19] electrodeposited [20], chemical vapor deposited [21] and DC magnetron sputtering [22] have been studied for last hundred years [9]. In the past optical and electrical properties of nickel oxide thin films have been studied extensively [23-27], but a little attention was waged towards the electrical and transport properties of pure nickel thin films. Similarly, according to best of our knowledge, there is a little evidence for the growth and study of magnetic properties of nickel thin film deposited on copper-substrates. Whal *et al* (2003) and J. Lamovec *et al* (2018) have reported the magneto-optical [28] and mechanical properties of nickel thin films deposited on copper substrates [29].

In this work, we have deposited nickel thin films on glass and copper substrates at different substrate temperature using pulse laser deposition (PLD) technique which is the most propitious exercise to develop the epitaxial thin films with suitable crystallographic direction [30]. The influence of substrate temperature on microstructural and structural parameters such as roughness, surface morphology, grain size and shape has been investigated. AFM, SEM, XRR and X-ray diffractometer (XRD) were utilized for study of surface morphology and microstructure of thin films. Magnetic, electrical and transport measurements of thin films were performed with Vibrating sample magnetometer (VSM) and Vander Pauw apparatus. The variation in coercive field (H_c), saturated magnetization (M_s) magnetic residual ratio, sheet resistance, and electrical resistivity of thin films with increased substrate-temperature are correlated to the structural and morphological changes. The effect of roughness, thickness and grain size on the % AMR, Hall mobility and carrier density has been discussed.

2. Experimental

Nickel thin films were deposited on the glass and copper substrates by pulsed laser deposition at T_s of 100°C, 300°C, 500°C and 100°C, 300°C, 500°C, 700°C respectively. The pressure in the deposition chamber was maintained at 1.1×10^{-7} mbar. A circular disc of pure nickel having thickness 3 mm and diameter 2 cm (provided by Test Bourne -Ltd, UK) was used as a target. The nickel target was irradiated with laser energy density of 2×10^{10} watt/cm² by fixing the wavelength and repetition rate of the Nd: YAG laser (Q-switch) at $\lambda=355\text{nm}$ and 10 Hz respectively. The glass and copper sheet of thickness 0.5 mm were cut into 10 mm × 10 mm square pieces which were used as substrates for the deposition of nickel thin films. The substrates were cleaned carefully by an ultrasonic bath in acetone for half an hour. They were then dried to remove the drops of solvent. Substrates were placed 4 cm away from the target during the deposition process of 45 min. The nickel target was irradiated by focusing the laser pulse energy with quartz convex lens ($f = 50\text{cm}$). The substrate and target were set in to continuous rotation.

3. Results and discussion

3.1. XRD analysis

The samples of nickel thin films were scanned in 2θ range of 20° - 90° by a beam of x-rays emitted from the Cu K α source having wavelength (λ) 1.54 Å . X-ray diffraction spectra of nickel thin film deposited on glass substrate is shown Fig. 1(a). The substrate temperature, $T_s = 100^\circ\text{C}$ supports the amorphous growth of thin film with no clear crystalline peak. The amorphous growth may be caused by low mobility of ad-atoms on substrate surface at low temperature. In the diffraction pattern of thin-film grown at 300°C, two nickel peaks (111) and (200) were appeared at 44.5° [31] and 52° [4,15], respectively. Low intensity peaks support the formation of weak nickel phase and polycrystalline structure of film at 300°C. Two intensive nickel peaks at 44.45° (111) and 52° (200) were appeared in the diffraction spectra of thin film deposited at 500 °C which confirms the crystalline growth of nickel.

Fig. 1(b) shows the XRD spectra of nickel thin film grown on Cu substrates. Three strong peaks (111), (200) and (200) at 43.20° , 50.44° and 74.15° , respectively, belong to the Cu-substrate [JCPDS - 04-0836 [32]. No nickel peak was observed in the diffracted spectra of nickel films at T_s of 100°C and 300°C . At lower T_s the ad-atoms deposited on substrate after travelling a short distance of few nanometers when arrived on substrate due to low kinetic energy and surface mobility which causes the amorphous growth of thin film. However, at T_s 500°C the ad-atoms with higher kinetic energy may obtain sufficient surface mobility on substrate to initiate the crystalline growth of the film. The presence of nickel peak at 44.45° [15,31] in the XRD pattern confirm its crystalline structure.

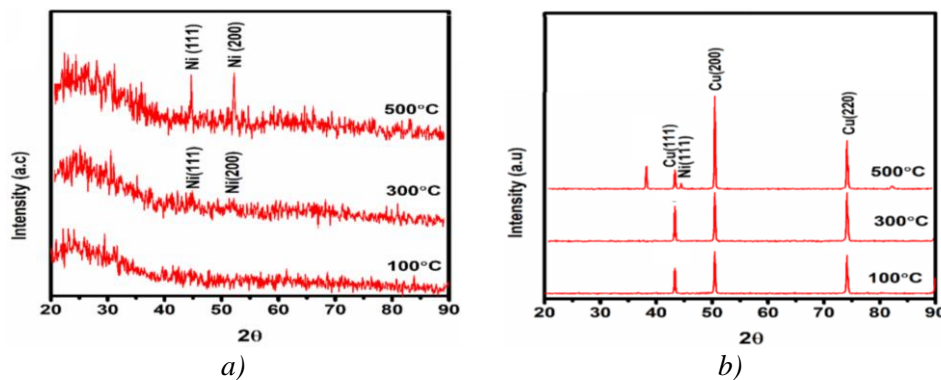


Fig. 1. XRD graphs of nickel thin films deposited on (a) glass and (b) copper substrates at $T_s = 100^\circ\text{C} - 500^\circ\text{C}$ using PLD

3.2 SEM analysis

A scanning electron microscope (SEM) was used to study the surface morphology of nickel thin films deposited on glass and Cu- substrates. SEM micrograph of thin-film grown at lower substrate temperature 100°C indicate the formation of smooth film, however, there exist small clusters and droplets in the microstructure of the film as shown in Fig. 2 (a) and (b). However, at substrate temperature of 300°C the size and density of grains were increased. At 500°C the film becomes smooth with polycrystalline structure as shown in Fig. 2 (c). Pores and voids were observed in the microstructure of film. The formation of voids may be supported by the diffusion of small particles/grains to larger ones due to high surface mobility at elevated growth temperature and leaving vacancies behind them.

SEM images of thin films deposited on copper at low T_s of $100^\circ\text{C}-300^\circ\text{C}$, show the inhomogeneous microstructure with high density of pores and voids as shown in Fig. 3 (a, b). At lower temperature ablated species/ad-atoms stick the substrate surface at place of their landing. Therefore, the low surface mobility of less energetic ad-atoms may cause formation of pores and voids in the texture of film. But at higher T_s of 500°C high surface mobility of ad-atoms initiate the smooth and homogeneous growth of film by reducing the density of voids and pores as indicated in Fig. 3 (c). Further increase in T_s (700°C) the mobility of ad-atoms increased by higher order which may increase the transport of depositing atoms on substrate. This effect causes amalgamation of small grains to large grains at higher temperature as indicated by Fig. 3(d).

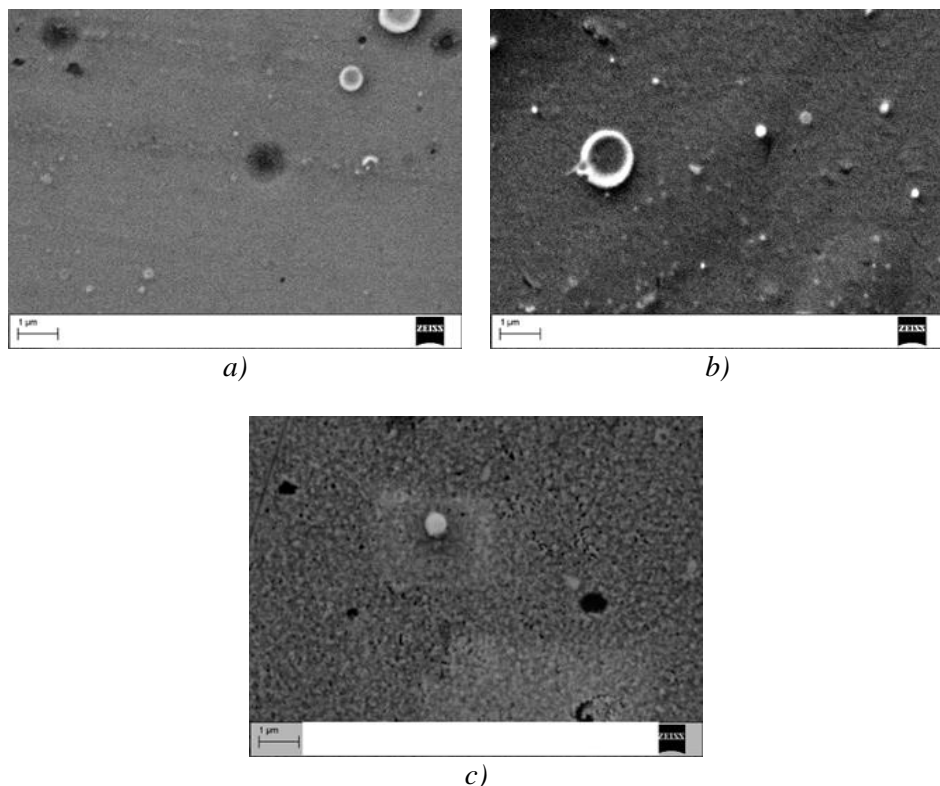


Fig. 2. SEM images of nickel thin films grown on glass-substrates at T_s of (a) $100\text{ }^{\circ}\text{C}$, (b) $300\text{ }^{\circ}\text{C}$ and (c) $500\text{ }^{\circ}\text{C}$.

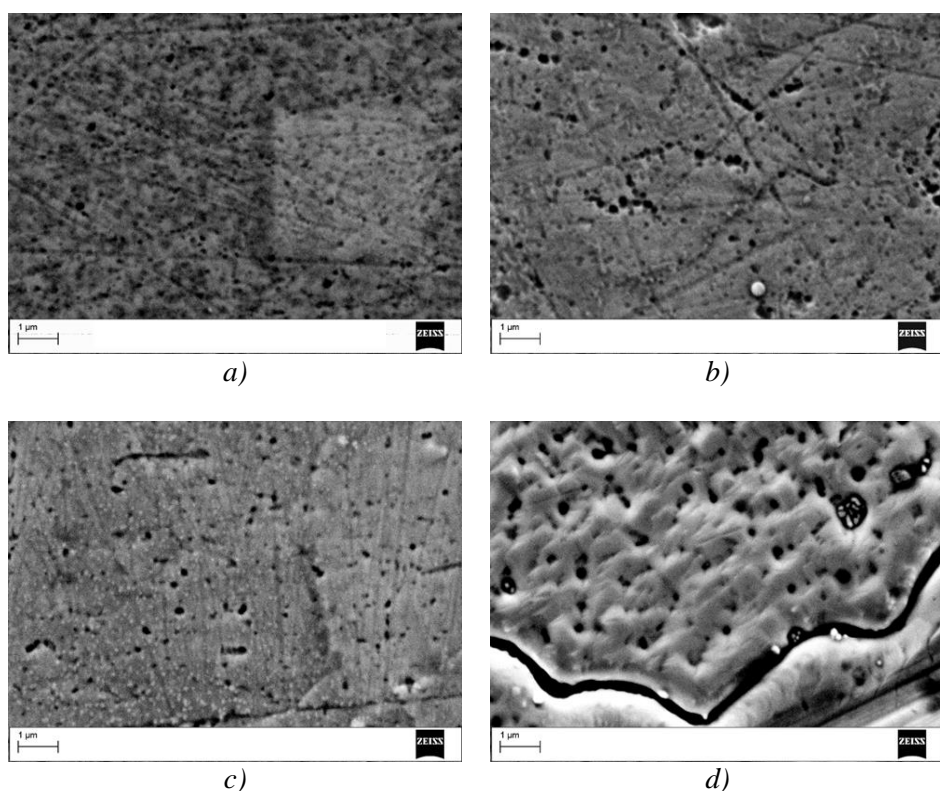


Fig. 3. SEM images of nickel thin films deposited on Cu-substrates at T_s of (a) $100\text{ }^{\circ}\text{C}$ (b) $300\text{ }^{\circ}\text{C}$ (c) $500\text{ }^{\circ}\text{C}$ and (d) $700\text{ }^{\circ}\text{C}$ using pulsed laser deposition.

3.3 AFM analysis

AFM image of thin film deposited on glass at lower substrate temperature 100 °C indicates the presence of some clusters and inhomogeneous growth of film was observed as shown in Fig. 4 (a). Lower surface mobility of ad-atoms causes formation of cluster in the microstructure of film at lower substrate- temperature. While at higher-growth temperature 300 °C, the density of cluster and droplets were appeared to be reduced. The grains with voids between their boundaries were observed in the microstructure of film as shown in Fig. 4 (b). The grains were coarsely distributed in the texture of the film. However, at T_S of 500 °C, large grains were transformed to grains of nearly the same size with voids at their centers. The smooth and homogeneous growth of thin -film initiated at 500 °C due to higher surface mobility as shown in Fig. 4(c). The estimated values of RMS roughness at T_S of 100 °C, 300 °C and 500 °C are 3 nm, 20 nm and 6 nm respectively.

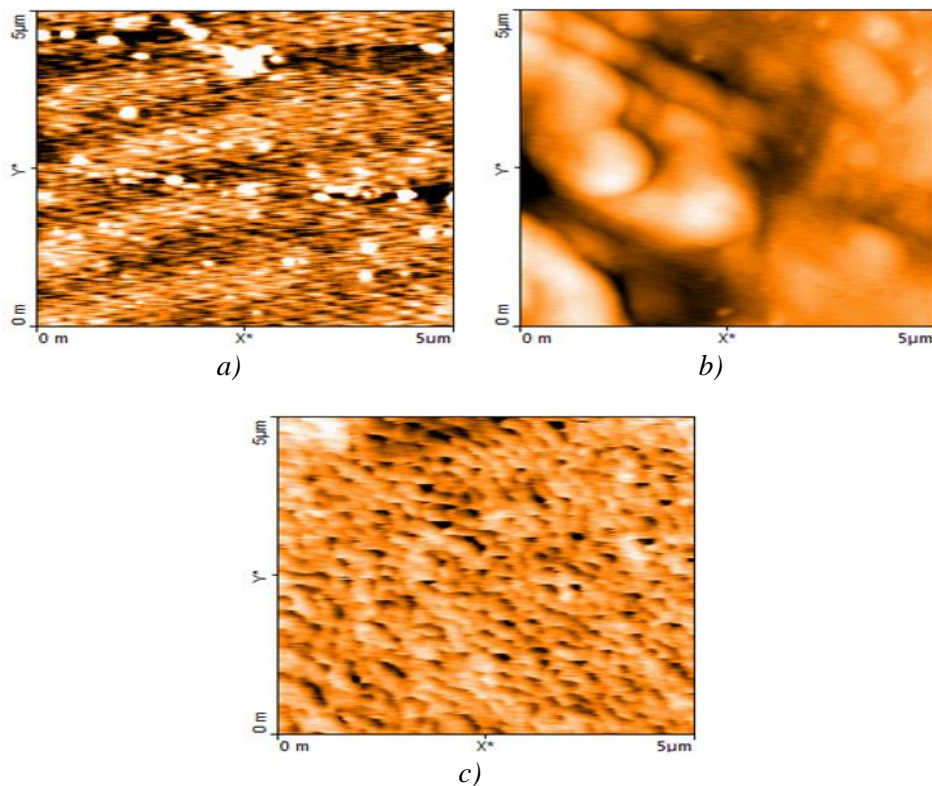


Fig. 4. AFM images of nickel thin films at T_S of (a) 100 °C (b) 300 °C and (c) 500 °C.

AFM image of thin film deposited on the Cu substrate at T_S of 100 °C, thin- film has non-uniform texture with presence of small grains and some voids as shown in Fig. 5 (a). At lower T_S the period of the atomic jump process of ad-atoms on the surface of substrate is large and mobility of ad-atoms on the surface is small, this effect leads to growth of non-uniform thin film. At T_S in range from 300 °C- 500 °C, the mobility of ad-atoms on the surface of substrate was increased and initiate the homogeneous growth of thin- film. AFM images of thin -film deposited at higher substrate temperature reveal that grain size of film was increased and grains of spherical shape with distinct grain boundaries were produced as indicated in Fig. 5 (b, c). At T_S 700 °C, the ad-atoms of higher surface mobility and potential energy have ability to overcome the nucleation potential of substrate surface and may be diffuse into Cu-substrate. Grain size and roughness of nickel thin films were also estimated using atomic force microscope. The estimated value of grain size of thin-film grown at T_S of 100 °C, 300 °C, 500 °C, and 700 °C are 360 nm, 600 nm, 666 nm and 1.6 μm and RMS roughness of thin film is 2 nm, 10 nm, 18 nm, 19 nm respectively.

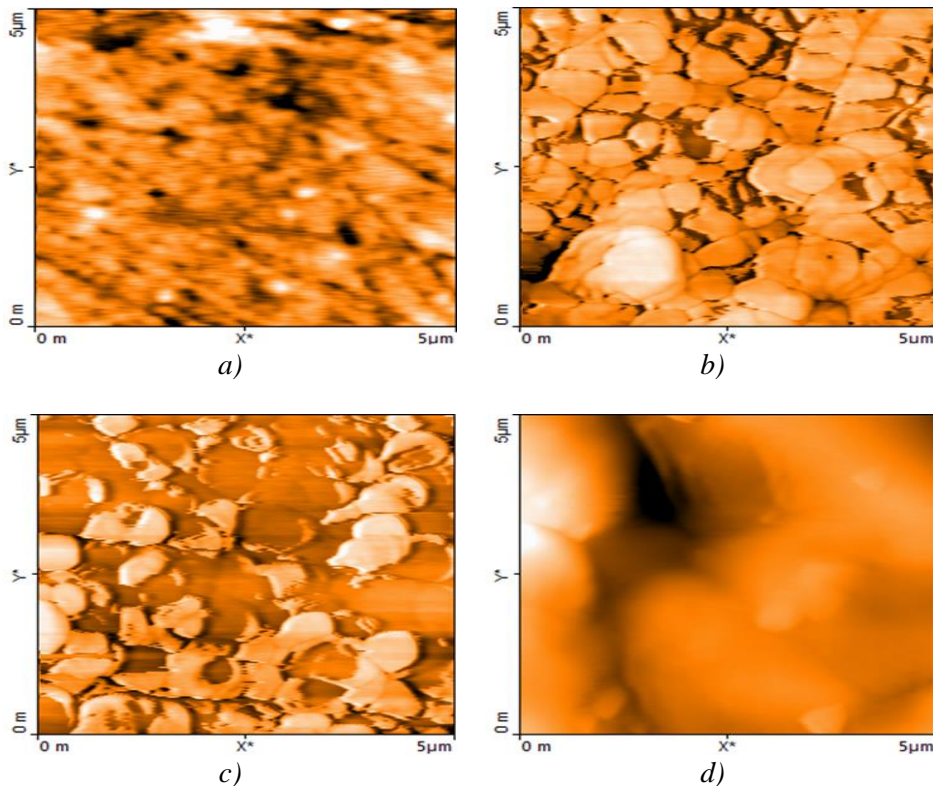


Fig. 5. AFM images of nickel thin films deposited on copper- substrates at T_s of (a) 100 °C (b) 300 °C (c) 500 °C and (d) 700 °C.

3.4. XRR analysis

X-ray reflectometry (XRR) was used to estimate the thickness of nickel thin films deposited on glass and copper -substrates. The estimated values of thickness of thin films deposited on glass substrate at T_s of 100 °C, 300 °C and 500 °C are 50 nm, 150 nm and 90 nm, while thickness of film deposited on copper-substrate at temperature of 100 °C, 300 °C, 500 °C, and 700 °C are 50 nm, 35 nm, 25 nm and 30 nm respectively. The values of thickness and RMS of the thin films deposited on glass and copper substrates are listed in Table 1.

Table 1. Thickness and roughness of Nickel thin films deposited on glass and copper substrates.

T_s (°C)	Glass-substrate		Cu-Substrate	
	Thickness (nm)	RMS Roughness (nm)	Thickness (nm)	RMS Roughness (nm)
100	50	3	50	2
300	150	20	35	10
500	90	6	25	18

3.5. Magnetic properties

Vibrating sample magnetometer (VSM) System (Lake Shore 7300 Series, USA) was used to generate magnetic data of thin films. The magnetic field was applied in-plane to sample of thin film for recording the $M-H$ loop. Magnetic characteristics such as saturated magnetization (M_s), coercivity (H_c), magnetic residual ratio and magnetic moment (M_r) were measured from the $M-H$ loop. The values of magnetic moment (M_r), magnetic residual ratio and coercivity (H_c) are plotted in Figures 6(a-c). The coercivity of thin films grown at 100 °C, 300 °C and 500 °C are 27.7 mT , 8.4 mT and 6.7 mT respectively while, magnetic moment and magnetic residual ratio of thin film deposited at 100 °C are 0.83 $\mu\text{A}\cdot\text{m}^2$ and 0.97. At T_s of 100 °C, roughness of film is 3nm therefore;

due to smaller roughness magnetic moment and saturated magnetization are large. At T_s of 300 °C, roughness of film increased from 2 nm-20 nm and leads to decrease in magnetic moment and saturated magnetization. The value of these parameters at 300 °C is 0.51 $\mu\text{A}/\text{m}$ and 0.25 $\mu\text{A}\cdot\text{m}^2$ respectively. At further higher temperature 500 °C roughness of film reduced from 20 nm- 6 nm. Therefore, M_s and Mr of thin-film were increased and their values become 0.71 $\mu\text{A}/\text{m}$ and 0.46 $\mu\text{A}\cdot\text{m}^2$ respectively. Magnetic properties are function of substrate temperature, substrate material roughness and thickness. Our results showed that at higher deposition temperature, roughness and thickness of thin film decreases and support the smooth and polycrystalline growth of film. The magnetic domains of film may easily aligned in the direction of applied magnetic field and are responsible for the increase in saturated magnetization (M_s) and magnetic moment (Mr).

M - H graphs of nickel thin films deposited on copper were drawn to measure magnetic parameters such as saturated magnetization (M_s) coercivity (H_c), magnetic residual ratio and magnetic moment (Mr). At T_s , 100 °C -300 °C magnetic parameters such as (H_c), (M_s) and magnetic residual ratio are large and then were significantly decreased with increase in substrate-temperature 100 °C -500 °C. At deposition temperature in range of 100 °C-700 °C, roughness of film was increased from 2 nm-20 nm while, thickness was reduced from 50 nm-30 nm respectively.

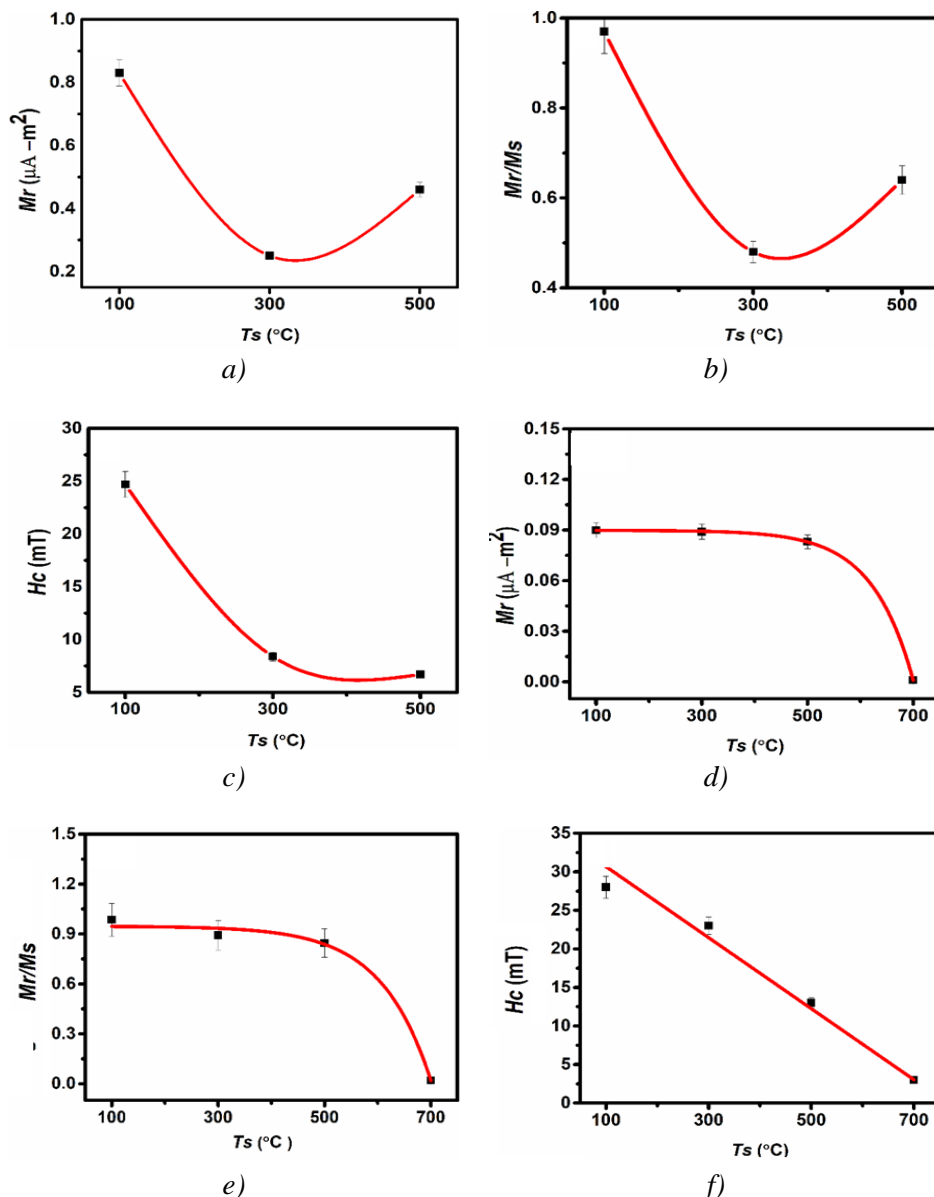


Fig. 6. Effect of T_s on the magnetic properties of nickel thin film deposited (a-c) on glass and (d-f) on copper substrates.

Magnetic properties of film are function of crystallinity, roughness, thickness and grain size. Therefore, for the smooth and homogeneous growth of thin-film, magnetic domains with in crystal structure tend to align in the direction of applied- field and lead to decrease the coercive field (H_c). Magnetic moment (Mr) of thin-film was decreased from $(0.90 \times 10^{-7} \text{ A-m}^2$ to $0.01 \times 10^{-7} \text{ A-m}^2$) with increase in T_s from $100 \text{ }^\circ\text{C}$ - $700 \text{ }^\circ\text{C}$ indicated in Fig. 6 (d). Similarly coercive field (H_c) and residual magnetic ratio were decreased 28 mT- 3 mT and 0.98-0.02 respectively with increase in T_s from $100 \text{ }^\circ\text{C}$ - $700 \text{ }^\circ\text{C}$ as illustrated in Fig. 6 (e,f) .The increase in roughness and grain size at higher temperature support the reduction in magnetic parameters.

3.6. Electrical properties

The Vander Pauw four-point method is the most common technique used for the measurement of the electrical and transport properties of thin films [33]. The electrical properties of thin films are function of deposition temperature, thickness, surface morphology, and roughness. The variation of sheet resistance and electrical resistivity with substrate temperature is illustrated in Fig. 7 (a) and (b) respectively. The electrical resistivity of thin film is $6.18 \times 10^{-6} \Omega\text{-m}$ at $T_s = 100 \text{ }^\circ\text{C}$ and was dropped to $0.526 \times 10^{-6} \Omega\text{-m}$ with increase in the substrate- temperature from $100 \text{ }^\circ\text{C}$ to $500 \text{ }^\circ\text{C}$. At lower growth temperature, grains are small with undistinguished boundaries and are randomly distributed in the texture of film. Therefore, due to amorphous growth and inhomogeneous microstructure, the electrical resistivity of film is higher. But at $T_s = 500 \text{ }^\circ\text{C}$, the structure of film become smooth and crystalline because of reduced thickness (150-90 nm). The smaller grains with their uniform distribution and polycrystalline growth which lead to decrease in roughness. The decrease in thickness, roughness, grain size and high order of crystallinity cause the decrease in the electrical resistivity of thin film at higher temperature.

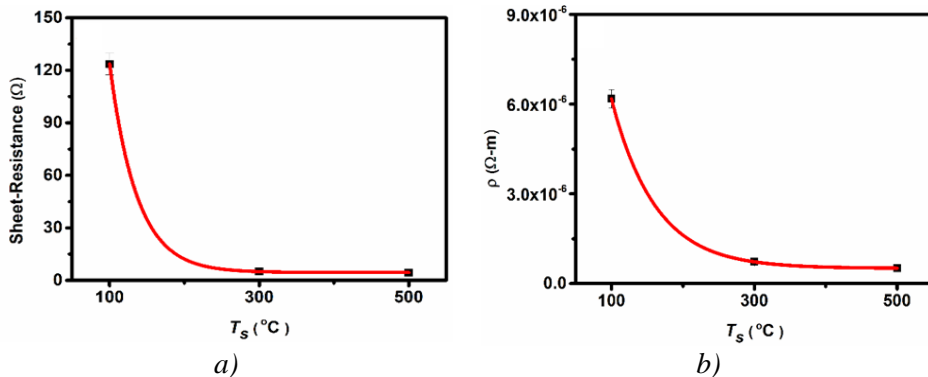


Fig. 7. Effect of T_s , on (a) sheet resistance (b) electrical resistivity of thin film deposited on glass-substrate.

3.7. Anisotropic-magnetoresistance (AMR)

The variation in the resistance of conducting materials under the influence of the magnetic field is called magnetoresistance. In case of ferromagnetic materials, this effect is called anisotropic magnetoresistance (AMR) because it depends on the orientation of magnetization with respect to the direction of current flowing through the material. AMR is anisotropic magnetoresistance and is used as a magnetic detector for a magnetic bubble and for digital recording. Thin films of ferromagnetic material are used for the fabrication of these delicate and small size detectors [34]. AMR of thin film was measured by Vander Pauw four- probe method. The magnetoresistance of thin film was increased at higher deposition temperature due to reduction in thickness and grain size. AFM images of thin film deposited at $500 \text{ }^\circ\text{C}$ showed that high density of grains in the texture as compared to film grown at lower temperature $100 \text{ }^\circ\text{C}$ - $300 \text{ }^\circ\text{C}$. Therefore, charge carriers suffer more collisions from the grain boundaries and cause the increase in magnetoresistance. The longitudinal and transverse anisotropic magnetoresistance (AMR) of nickel thin films deposited at T_s from 100°C to 500°C lies in the range 0.003- 0.98 and 0 - 1.32 as shown in Fig. 8 (a) and (b) respectively. Our results showed that anisotropic magnetoresistance are close to each other in experiments conducted in both the longitudinal and transverse modes.

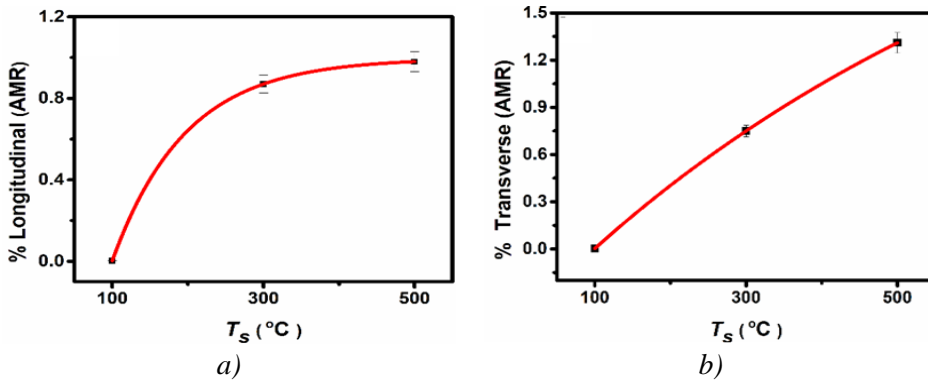


Fig. 8. The variation of longitudinal and transverse % AMR of nickel thin films vs T_s

3.8. Hall measurements

Carrier mobility of materials is a fundamental property which describes how easy or difficult carriers charge gives a response to the applied electric field. It also gives information about the phenomenon of scattering of carriers from the material. Carrier mobility and carrier density of thin-film determine its resistivity which is an intrinsic property.

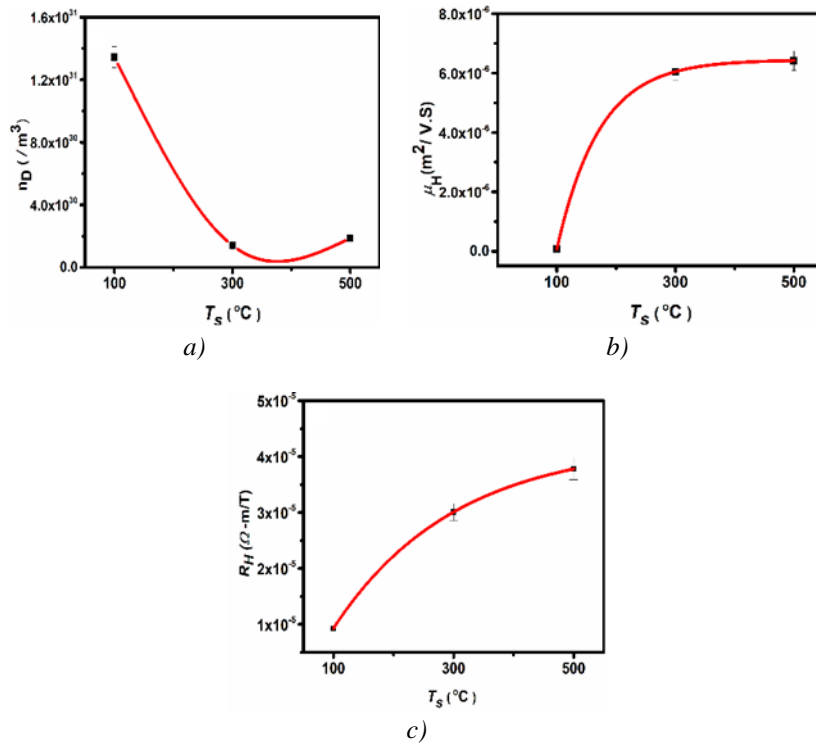


Fig. 9. Variation of carrier density, carrier mobility and Hall coefficient of nickel thin-films deposited on glass substrates at T_s of (a) 100 $^{\circ}\text{C}$, (b) 300 $^{\circ}\text{C}$ and (c) 500 $^{\circ}\text{C}$.

Resistivity, carrier density and carrier mobility are related by $\rho = 1/n e \mu$. Where, n is the carrier density, d is thickness, e is fundamental charge and μ is the carrier mobility. The relation between Hall coefficient (R_H), carrier mobility (μ_H), carrier density (n_{3D}) and resistivity of thin film are given by equations 1-3 [33].

$$R_H = \frac{1}{n e} \quad (1)$$

$$\mu_H = R_H / \rho \quad (2)$$

$$n_{3D} = n_s / d \quad (3)$$

The effect of substrate temperature on the number density, carrier mobility and Hall coefficient is illustrated in Fig. 9 (a), (b) and (c) respectively. By using above equations (R_H), (μ_H) and (n_{3D}) of thin films were calculated. Hall mobility of thin-film was increased from $0.07 \times 10^{-6} \text{ m}^2/\text{V.s}$ to $6.42 \times 10^{-6} \text{ m}^2/\text{V.s}$ at growth- temperature in range from 100°C - 500°C , while carrier density (n_{3D}) was decreased from $13.44 \times 10^{30}/\text{m}^3$ to $1.87 \times 10^{30}/\text{m}^3$. At higher growth temperature Hall-coefficient (R_H) was increased from $0.93 \times 10^{-5} \Omega\text{-m} / \text{T}$ to $3.78 \times 10^{-5} \Omega\text{-m} / \text{T}$ which may be due to presence of pores and voids in the microstructure of film as confirmed by AFM and SEM images.

4. Conclusion

Using pulsed laser deposition, nickel thin films were deposited on the glass and copper-substrates. X-ray diffraction patterns of thin films deposited on glass-substrates showed the amorphous growth of film at lower T_s (100°C), while polycrystalline growth started at T_s of 300°C . The homogeneous and crystalline growth of strong nickel phase was observed at 500°C . Surface morphology revealed that roughness and thickness of film deposited at T_s of 300°C reached to 20 nm and 150 nm respectively and then reduced to 6 nm and 50 nm at 500°C due to improvement in crystallinity and high surface mobility of ad-atoms on substrate surface. Magnetic moment (M_r), and coercive field (H_c) were decreased from $0.83 \mu\text{A}\text{-m}^2$ - $0.46 \mu\text{A}\text{-m}^2$, 27.7 mT to 6.7 mT respectively at temperature range of 300°C - 500°C . The electrical resistivity and carrier density were decreased $6.18 \times 10^{-6} \Omega\text{-m}$ to $0.526 \times 10^{-6} \Omega\text{-m}$ and $13.44 \times 10^{30}/\text{m}^3$ to $1.87 \times 10^{30}/\text{m}^3$ respectively, while Hall coefficient (R_H) and carrier mobility (μ_H) were increased at higher T_s . The X-ray diffracted patterns for the nickel thins film grown on copper- substrates indicated the amorphous growth at T_s in range of 100°C - 300°C and transform in to crystalline structure at T_s of 500°C . Grain size was increased from 360 nm to 1.6 μm , roughness was increased from 2 nm to 19 nm; however, film thickness was decreased from 50 nm-25nm. Similarly, magnetic moment (M_r) was reduced from $0.90 \times 10^{-7} \text{ A}\text{-m}^2$ to $0.01 \times 10^{-7} \text{ A}\text{-m}^2$ and coercive field (H_c) was reduced from 28 mT to 3 mT.

Acknowledgements

This research work is partially supported by Higher Education Commission (HEC) of Pakistan Project No. 20-1868/R&D/105754. M. Nawaz Rizwan acknowledge HEC Pakistan for financial support of six months visit to University of the Bristol, UK under international research support initiative programme (IRSIP).

References

- [1] Pouyan Motamed, Ken Bosnick, Kai Cui, Kenneth C. Cadien, James Hogan, ACS Applied Materials & Interfaces **9**(29), 24722 (2017).
- [2] Ali Behroozfar, Md. Emran Hossain Bhuiyan, Soheil Daryadel, David Edwards, Brian J. Rodriguez, Majid Minary-Jolandan, Nanotechnology **31**(5) 055301 (2020)
- [3] Gauthier Lefevre, Sébastien Saitzek, Florent Blanchard, Anthony Ferri, Pascal Roussel, Rachel Desfeux, Adlane Sayede, CrystEngComm **20** (34), 1 (2018).
- [4] Thomas Otito, Georges-Ivo Ekosse, Sathiaraj, T. Stephen, Journal of Applied Sciences **11**(2), 57 (2007).
- [5] J. Potocnik, M. Nenadovic, B. Jokic, S. Strabac, Z. Rakocevic, Science of Sintering **45**, 61 (2013).
- [6] H. Gleiter, Acta Materials **48** 1 (2000).

- [7] M. E. McHenry, D. E. Laughlin, *Acta Materials* **48**, 223 (2000).
- [8] H. Gleiter, *Progress in Materials Science* **33**, 223 (1989).
- [9] Hamidreza Hajihoseini, Movaffaq Kateb, Snorri Þorgeir Ingvarsson, Jon Tomas Gudmundsson, *Beilstein Journal of Nanotechnology* **10**, 1914 (2019).
- [10] Y. Pauleau, S. Kukielka, W. Gulbinski, L. Ortega and S. N. Dub, *Journal of Physics D: Applied Physics* **39**, 2803 (2006).
- [11] V. V. Atuchin, T. I. Grigorieva, L. D. Pokrovsky, V. N. Kruchinin, D. V. Lychagin, C. V. Ramana, *Modern Physics Letters B* **26**(5), 1150029 (2012).
- [12] M. Adsén, R. Joerger, K. Jarrendahl, E. Wackelgard, *Solar Energy* **68**, 325 (2000).
- [13] Prashant Kumar, *Nanoscale Research Letters* **5**, 1596 (2010).
- [14] J. Potocnik, M. Nenadovic, N. Bundaleski, B. Jokic, M. Mitric, M. Popovic, Z. Rakocević, *Materials Research Bulletin* **84**, 455 (2016).
- [15] Amrut S. Lange, Satish J. Sharma, Ramchandra B. Pode, *Archives of physics research* **1**, 49 (2010).
- [16] B. Geetha Priyadarshini, S. Aich, M. Chakraborty, *Journal of Materials Science* **46**, 2860 (2011).
- [17] N. Radic, P. Dubcek, S. Bernstorff, I. Djerdj, A. M Tonejc, *Journal of Applied Crystallography* **40**, 377 (2007).
- [18] Michel Becht, Fachri Atamny, A. Baiker, Klaus-Hermann Dahmen, *Surface science* **371**, 399 (1997).
- [19] Prashant Kumar, M. Ghanashyam Krishna, A. K Bhattacharya, *Bulletin of Materials Science* **32**(3) 263 (2009).
- [20] S. B. Pandeya, D. Das, A. K. Kar, *Applied Surface Science* **337** 195 (2015).
- [21] N. Li, S. Schaffer, R. Datta, T. Mewes, T. M. Klein, A. Gupta, *Applied Physics letters* **101**, 13240 (2012).
- [22] J. B. Yi, Y. Z. Zhou, J. Ding, G. M. Chow, Z. L. Dong, T. White, Xing Yu Gao, A. T. S. Wee, X. J. Yu, *Journal of Magnetism and Magnetic Materials* **284**, 303 (2004).
- [23] A. Madhavi, Ch. Sesbendra Reddy, N. V. Ravindra, P. Lokeshand, *International Journal of advance research in Physical science* **1**(4), 16 (2014).
- [24] A. Madhavi, G.S Harish, P. Sreedhara. Reddy, *International journal of science technology and engineering* **2**(11), 742 (2016).
- [25] Hao-Long Chen, Yang-Ming Lu, Wing-Sing Hwang, *Materials Transaction* **46**(4), 872 (2005).
- [26] Marek Guziewicz, Jakub Grochowski, Michal Borysiak, Elana Kaminska, Jaroslaw Domagala, Witold Rzodkiewicz, Bartlomiej S. Witkowski, Krystyna Golaszewska, Renata Kruszka, Marek Ekielski, Anna Piotrowska, *Optica Applicata* **XLI**(2), 431 (2011).
- [27] Chanae Park, Juhwan Kim, Kangil Lee, Suhk Kun Oh, Hee Jae Kang, Nam Seok Park, *Applied Science and Convergence Technology* **24**(3), 72 (2015).
- [28] M. Wahl, Th. Herrmann, N. Esser, W. Richter, *Physica Status Solidi* **0**(8), 3002 (2003).
- [29] Jelena Lamovec, Ivana Mladenović, Vesna Jović, Vesna Radojević, Stevo Jaćimovski, Goran Jovanov, *Zastita Materijala* **59**(3), 394 (2018).
- [30] T. Zeehan , S. Anjum, S. Waseem, M. Riaz, R. Zia, *Digest Journal of Nanomaterials and Biostructures* **14**(4) 855 (2019)
- [31] Yuanqing He, Xuegeng Li, Mark Swihart, *Chemistry of Materials* **17**, 1017 (2005).
- [32] T. Theivasanthi, M. Alagar, <https://arxiv.org/abs/1003.6068> (2010).
- [33] Toru Matsumura, Yuichi Sato, *Journal of Modern Physics* **1**, 340 (2010).
- [34] T. R. McGuire, R. I, *IEEE Transaction on magnetics Potter* **MAG-1**, 1038 (1975).